ACS APPLIED MATERIALS & INTERFACES

Research Article

www.acsami.org

Hierarchical Nanocomposites of Vanadium Oxide Thin Film Anchored on Graphene as High-Performance Cathodes in Li-Ion Batteries

Zhe-Fei Li,[†] Hangyu Zhang,[‡] Qi Liu,[†] Yadong Liu,[†] Lia Stanciu,[‡,§] and Jian Xie*,[†]

[†]Department of Mechanical Engineering, Indiana University-Purdue University Indianapolis, Indianapolis, Indiana 46202, United States

[‡]Weldon School of Biomedical Engineering and [§]School of Materials Engineering, Purdue University, West Lafayette, Indiana 47907, United States

Supporting Information

ABSTRACT: Hierarchical nanocomposites of V_2O_5 thin film anchored on graphene sheets were prepared by slow hydrolysis of vanadyl triisobutoxide on graphene oxide followed by thermal treatment. The nanocomposite possessed a hierarchical structure of thin V_2O_5 film uniformly grown on graphene, leading to a high specific surface area and a good electronic/ionic conducting path. When used as the cathode material, the graphene/V_2O_5 nanosheet nanocomposites exhibit higher specific capacity, better rate performance, and longer cycle life, as compared to the pure V_2O_5. The nanocomposite cathode was able to deliver a specific capacity of 243 mAh/g, 191 mAh/g, and 86 mAh/g at a current density of 50 mA/g, 500 mA/g, and 15 A/g, respectively. Even after 300 cycles at 500 mA/g, the composite electrode still exhibited a specific capacity of ~122 mAh/g, which corresponds to ~64% of its initial capacity. This enhanced electrochemical performance can be attributed to facile electron transport between graphene and V_2O_5, fast Li-ion diffusion within the electrode, the high surface area of the composites, and a pore structure that can accommodate the volume change during lithiation/delithiation, which results from the unique hierarchical nanostructure of the V_2O_5 anchored on graphene.

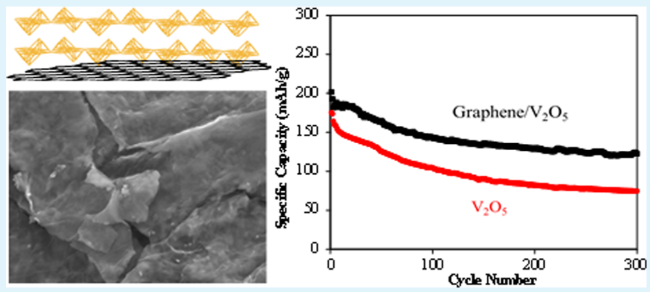

KEYWORDS: *graphene, V_2O_5, nanosheets, hierarchical, Li-ion battery, cathode*

INTRODUCTION

The increase in energy consumption demands energy storage devices with high energy and power density. Over the past few decades, lithium-ion batteries (LIBs) have achieved great success in portable electronics applications. However, the wide use of LIBs in electric and hybrid vehicles is limited by the low energy and power density of current commercial LIBs. Common traditional cathode materials like $LiFePO_4$, $LiCoO_2$, and $LiMn_2O_4$ can only deliver specific capacities less than 170 mAh/g.[1] Therefore, much attention has been devoted to developing high-capacity cathode materials.[2] Among promising candidate cathode materials, V_2O_5 has been extensively studied due to its abundance, low cost, high specific capacity, and energy density.[3−5] Theoretically, V_2O_5 can accommodate up to three lithium ions, corresponding to a specific capacity of 442 mAh/g (assuming three electrons insertion/deinsertion) or 294 mAh/g (assuming two electrons insertion/deinsertion).[6] However, V_2O_5 suffers from several intrinsic flaws (i.e., slow diffusion of Li ions, low electronic conductivity, and irreversible structural changes during cycling), leading to poor rate capability and cycling stability.[7−10]

During the past decades, much effort has been made to overcome these drawbacks. To enhance the diffusion of Li ions within V_2O_5, various V_2O_5 nanostructures have been prepared, such as V_2O_5 nanofibers,[11] nanotubes,[12] nanosheets,[13] and hollow spheres.[14,15] Particularly, two-dimensional (2D) nanosheet materials like $VOPO_4$ and $LiFePO_4$ have been shown to possess excellent electrochemical properties due to the fast charge transfer and short diffusion path.[16,17] Combining V_2O_5 with electronically conductive materials can increase the conductivity of V_2O_5 and suppress the irreversible capacity loss due to volume change.[18−21] Among these candidate carbonaceous materials, graphene, a single atomic layer of sp^2 hybrid carbon atoms, has attracted tremendous attention due to its high specific surface area, electrical conductivity, and mechanical strength.[22] Specifically, the 2D nanosheet structure of graphene can provide a fast electron conduction path for V_2O_5. In addition, graphene nanosheets possess a high electroactive surface, which facilitates the diffusion of electrolyte ions and increases the size of the contact area available to the electrolyte. Recently, graphene has been incorporated into various V_2O_5 nanostructures, such as V_2O_5 spheres,[23] V_2O_5 nanowires,[24] V_2O_5 xerogels,[25] V_2O_5 nanoribbons,[26] and self-assembled vertically grown V_2O_5 nanosheets.[27]

Received: July 18, 2014
Accepted: October 8, 2014
Published: October 8, 2014

   dx.doi.org/10.1021/am5047262 | ACS Appl. Mater. Interfaces 2014, 6, 18894−18900

Here, we demonstrate a facile method to prepare V_2O_5 thin film anchored on graphene via a controlled hydrolysis approach. The resulting nanocomposites consist of V_2O_5 nanosheet-like structure hierarchically grown on the graphene sheets. When used as a cathode in Li-ion batteries, the graphene/V_2O_5 nanocomposites exhibited high specific capacity, high rate capability, and high cycling stability, as compared to the pure V_2O_5. The enhanced electrochemical performance can be attributed to the maximized synergetic effect of the graphene and V_2O_5.

2. EXPERIMENTAL SECTION

2.1. Synthesis of Graphene Oxide. Graphene oxide (GO) was prepared following the previously published procedures.[28,29] Natural graphite flakes were preoxidized before oxidation by the Hummers' method. Then, 2 g of preoxidized graphite, 1 g of sodium nitrate, and 46 mL of sulfuric acid were mixed and stirred for 15 min in a 500 mL flask immersed in an ice bath. Potassium permanganate (6 g) was slowly added to the above suspension. After 15 min, the temperature was heated to ~35 °C and maintained at that temperature for 30 min. Then 92 mL of deionized (DI) water was added dropwise to the suspension, causing a violent effervescence. The temperature was maintained above 98 °C for 30 min. The suspension was diluted by 280 mL of water and treated with 10 mL of 30% H_2O_2 to reduce the unreacted potassium permanganate. The GO was washed successively with 1 M HCl solution and DI water by centrifugation several times to remove residual salts and acids. The obtained GO was sonicated to achieve a stable GO dispersion in DI water. Then, the GO dispersion solution was subjected to another centrifugation at 5000 rpm for 5 min to remove the unexfoliated GO. Finally, the GO was freeze-dried.

2.2. Synthesis of Graphene/V_2O_5 Composites. GO (100 mg) and vanadyl triisobutoxide (1.2 mL) were dispersed in 100 mL of anhydrous *N*-methyl-2-pyrrolidone (NMP) by ultrasonication to produce a V-precursor/GO dispersion solution. The dispersion was continuously stirred under Ar atmosphere for 24 h to form a monolayer of V_2O_5 on GO via the reaction with hydroxyl and carboxyl groups on GO.[20,30] Then, a mixture of NMP and water (10 mL, 1:1 v/v) was slowly added dropwise. The dispersion was stirred for another 24 h under ambient conditions, which resulted in the further nucleation of V_2O_5 on the V_2O_5 monolayer-functionalized GO. The resulting composites were precipitated by centrifugation at 10000 rpm, washed with acetone and water, and dried in a vacuum oven. Finally, the composites were heated at 300 °C for 2 h in air to crystallize the V_2O_5 and reduce GO to graphene.[31] For comparison, pure V_2O_5 was prepared following the same procedure without the addition of GO.

2.3. Characterization. X-ray photoelectron spectroscopy (XPS) was measured on a Kratos AXIS Ultra X-ray photoelectron spectrometer. Raman spectra were taken by a Craic Tech spectrometer with laser excitation at 785 nm. Thermal gravimetric analysis (TGA) curves were obtained using the TA Instrument SDT Q600. The morphology was characterized by a Philips CM 200 transmission electron microscope (TEM) and a JEOL-7800 scanning electron microscopy (SEM). The N_2 adsorption/desorption isotherms were determined by a Quantachrome Autosorb-iQ analyzer at 77 K. The Brunauer−Emmett−Teller (BET) specific surface area was calculated using adsorption data at the relative pressure range of 0.05−0.3. The total pore volumes were estimated from the amount adsorbed at a relative pressure (P/P_0) of 0.99. The Barrett−Joyner−Halenda pore size distribution was calculated based on the desorption branch of the isotherm.

2.4. Electrode Fabrication and Electrochemical Test. The electrochemical performance was characterized in a 2016-type coin cell. A lithium foil was used as the counter electrode. The working electrode was fabricated by pasting the slurry onto Al foil using the doctor-blade method. The slurry contained 75% active materials, 10% SuperP, and 15% poly(vinylene difluoride) in 1-methyl-2-pyrrolidinone (NMP). The electrode was dried in a vacuum oven at 80 °C overnight and then assembled into the coin cell in an Ar-filled glovebox (MBraun, <0.1 ppm of O_2 and <0.1 ppm of H_2O). The mass loading of the active material on each electrode was ~1.5 mg/cm^2. The electrolyte used was 1.2 M $LiPF_6$ in ethylene carbonate/ethyl methyl carbonate (3:7 v/v), and a Celgard polypropylene membrane was used as the separator. The galvanostatic charge/discharge tests were performed on an Arbin battery test station. Cyclic voltammetry (CV) and electrochemical impedance spectroscopy (EIS) were performed using the Solartron system (1287 + 1260).

3. RESULTS AND DISCUSSION

The possible formation mechanism is that the functional groups on GO (i.e., hydroxyl, carboxyl, epoxide) can serve as the polymerization sites of vanadyl triisobutoxide and nucleation sites. First, vanadyl triisobutoxide was anchored onto GO via condensation reaction with OH and COOH groups. During the controlled hydrolysis, V_2O_5 was formed on GO surface and in the solution through the olation and oxolation. Finally, further nucleation occurred on the formed V_2O_5, resulting in the hierarchical graphene/V_2O_5 nanocomposites. The morphology and structure of the as-prepared graphene/V_2O_5 hierarchical nanostructures were characterized by SEM and TEM. As shown in Figure 1a,b, a layered structure can be observed from the SEM image of both graphene and the graphene/V_2O_5 composites. It can be seen that the graphene/V_2O_5 sheets are much thicker than pure graphene. It is statistically estimated that the thickness of the V_2O_5 nanosheet or thin film is ~20−25 nm. Also, the surfaces of the graphene/V2O5 sheets are rougher due to the formation of V_2O_5. These V_2O_5 seem to be uniformly sandwiched between graphene sheets or deposited on graphene surfaces. The composition and element distribution of the composites can be obtained by energy dispersive X-ray spectroscopy (EDS) mapping images of carbon, vanadium, and oxygen in the graphene/V_2O_5 composite. It can be seen from Figure 1c that the distribution of carbon, vanadium, and oxygen is very uniform, indicating homogeneous dispersion of V_2O_5 on the graphene. TEM images in Figure 2a further show that the V_2O_5 nanosheet-like structures are coated on the graphene sheets over a large area in the nanocomposite. The high-resolution TEM image (Figure 2c) clearly shows crystal lattices with a *d*-spacing of 0.44 nm, corresponding to (001) planes of the crystalline orthorhombic phase of V_2O_5.[32]

Raman spectra of V_2O_5 and graphene/V_2O_5 were taken and are shown in Figure 3a. Two characteristic peaks of graphene (the D band at 1330 cm^{-1} and the G band at 1600 cm^{-1}) and the typical peaks of V_2O_5 (~404, 530, 700, and 990 cm^{-1}) were observed for graphene/V_2O_5 nanocomposites. It is worth noting that the Raman peaks of V−O (700 and 530 cm^{-1}) shifted slightly to a lower wavenumber, indicating that there exists a strong interaction between V_2O_5 and graphene due to the charge transfer.[33,34] It is also possibly due to the presence of a small amount of V^{4+}. Graphene/V_2O_5 was studied by XPS, and its V 2p spectrum is shown in Figure 3b. Two major peaks at ~517.8 and 525.2 eV can be ascribed to the V $2p_{3/2}$ and V $2p_{1/2}$ of V^{5+}. In addition, two small peaks near 516.5 and 524 eV can be found, corresponding to the presence of V^{4+}.[35] The molar ratio of V^{4+}/V^{5+} is ~7%. This may be caused by the incomplete oxidation of V_2O_5 or the charge transfer from graphene to V_2O_5. X-ray diffraction (XRD) patterns of graphene/V_2O_5 composites in Figure 3c can be attributed to the crystalline orthorhombic phase of V_2O_5.[36] However, the diffraction peak of graphene at ~24° was not observed in the diffraction pattern, probably due to its overlapping with (110) the peak of V_2O_5. It is also possible that V_2O_5 are uniformly distributed on graphene, preventing the

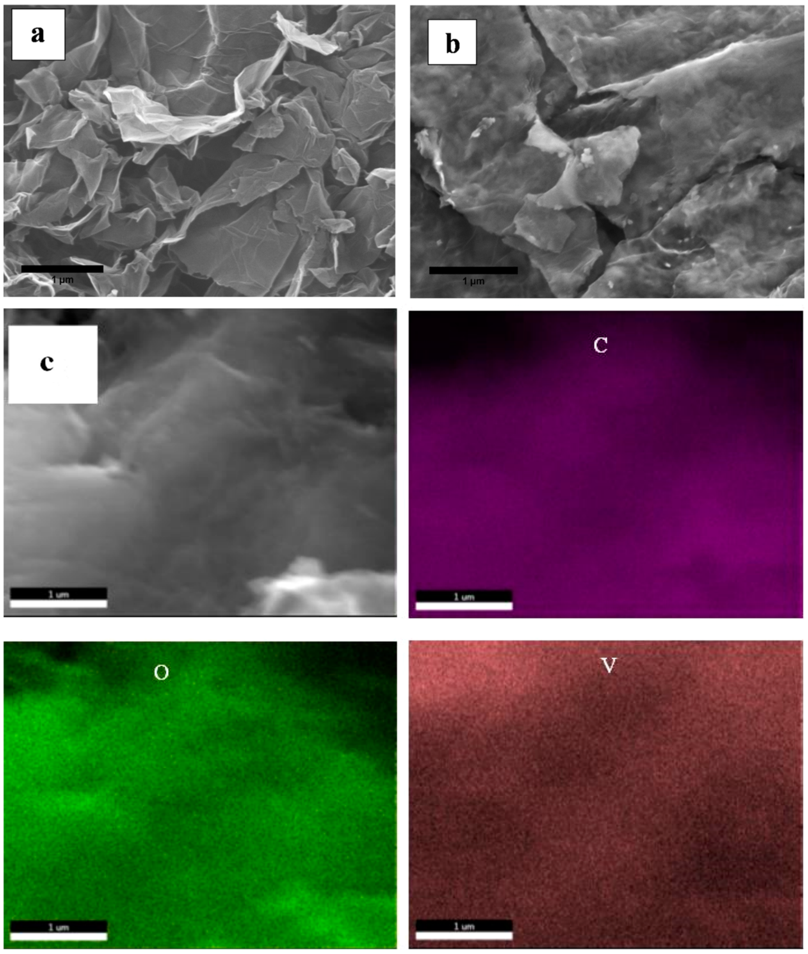

Figure 1. (a, b) SEM images of graphene/V_2O_5 nanocomposites (V_2O_5, as the red arrows indicate; graphene sheet wrinkles, as the black arrows indicate). (c) EDS mapping of C, O, and V elements in the graphene/V_2O_5 nanocomposites.

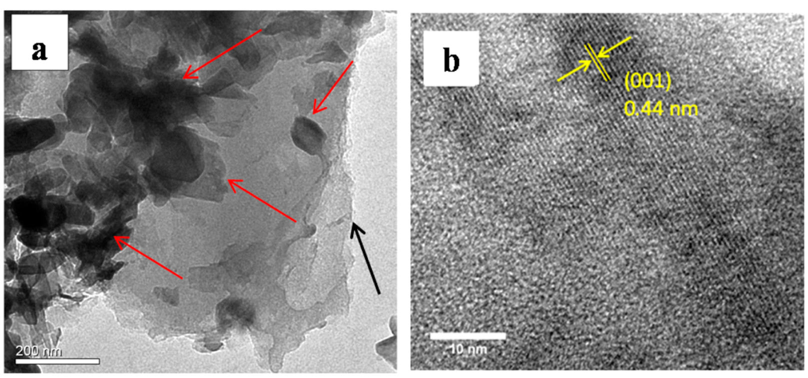

Figure 2. (a) Low-resolution and (b) high-resolution TEM images of graphene/V_2O_5 nanocomposites (V_2O_5, as the red arrows indicate; graphene sheet wrinkles, as the black arrows indicate).

restacking of the graphene sheets.[37] In short, the Raman, XPS, and XRD results illustrate the successful deposition of crystalline orthorhombic V_2O_5 on graphene.

The surface area, pore volume, and pore size of the samples are characterized by N_2 adsorption and desorption measurements and shown in Figure 4. The surface area is calculated by the BET method. The graphene/V_2O_5 nanocomposites nanocomposite has a specific surface area of 123 m^2/g, which is much higher than that of pure V_2O_5 (12 m^2/g). The graphene/V_2O_5 nanocomposites also possessed a larger pore volume and average pore size than pure V_2O_5 (Figure 4b). A large specific surface area can provide more contact area with the electrolyte, which can benefit the electrolyte ion transport within the electrode and improve electrochemical performance.

To evaluate the electrochemical lithium storage properties of the graphene/V_2O_5 nanocomposite as the cathode material of LIBs, a series of electrochemical measurements were carried out. Figure 5 shows cyclic voltammograms (CV) of the graphene/V_2O_5 nanocomposite at a scan rate of 0.5 mV/s in the voltage range of 2−4 V. Similar to pure V_2O_5, three major cathodic peaks appear in the CV curves at potentials of 3.35, 3.16, and 2.24 (vs Li/Li^+), corresponding to the phase transformations from α-V_2O_5 to β-$Li_{0.5}V_2O_5$, δ-LiV_2O_5 and γ-$Li_2V_2O_5$, respectively.[10,21,38]

dx.doi.org/10.1021/am5047262 | ACS Appl. Mater. Interfaces 2014, 6, 18894−18900

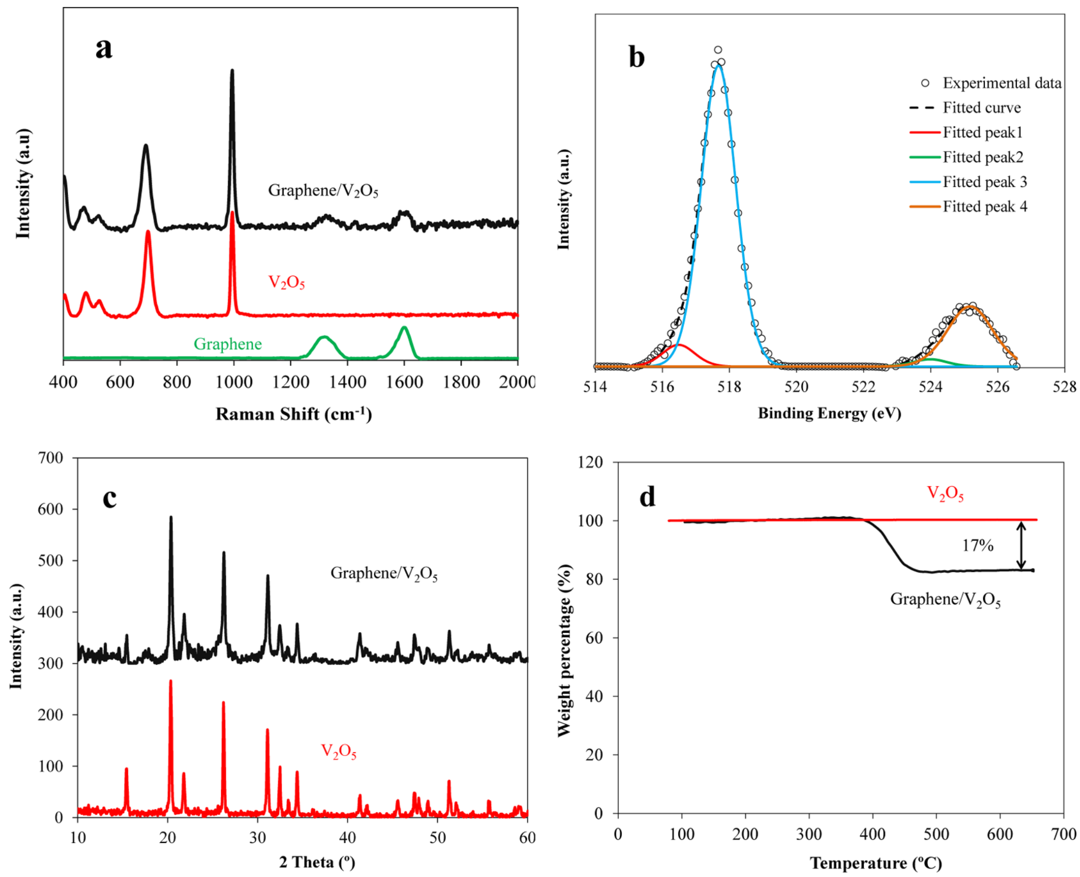

Figure 3. (a) Raman and (b) XPS spectra, (c) XRD patterns, and (d) TGA curves of V_2O_5 and graphene/V_2O_5.

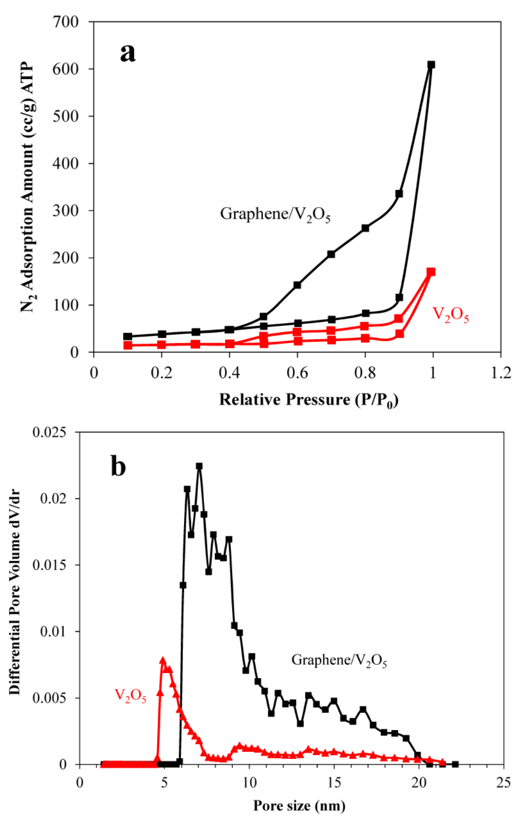

Figure 4. (a) N_2 adsorption/desorption isotherm and (b) pore size distribution of V_2O_5 and graphene/V_2O_5 nanocomposites.

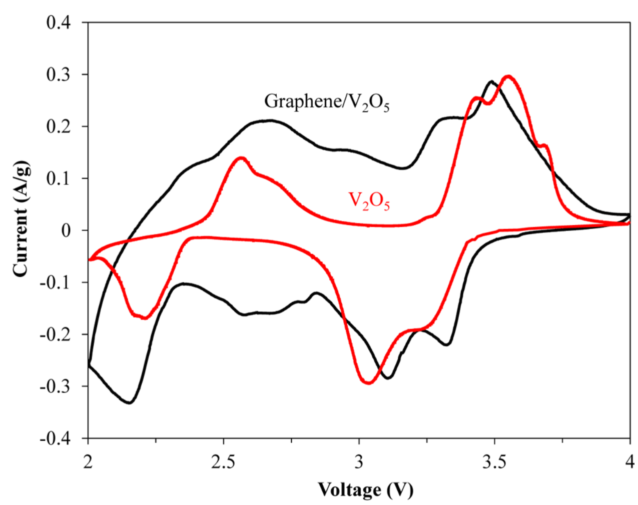

Figure 5. Cyclic voltammograms of the graphene/V_2O_5 nanocomposite electrode at a scan rate of 0.5 mV/s.

In addition, several small peaks between 2.5 and 2.9 V may be attributed to the lithiation/delithiation of amorphous V_2O_5 or the lower-valence vanadium oxide.[35,39] It can also be seen that the double-layer capacitance of graphene/V_2O_5 nanocomposites is higher than pure V_2O_5, suggesting a larger surface area of graphene/V_2O_5 nanocomposites.

Figure 6a presents the charge/discharge profiles of the graphene/V_2O_5 nanocomposite in the first and second cycles at a current density of 50 mA/g. The discharge/charge processes displays multiple redox plateaus between 2 and 4 V, similar to the

dx.doi.org/10.1021/am5047262 | ACS Appl. Mater. Interfaces 2014, 6, 18894−18900

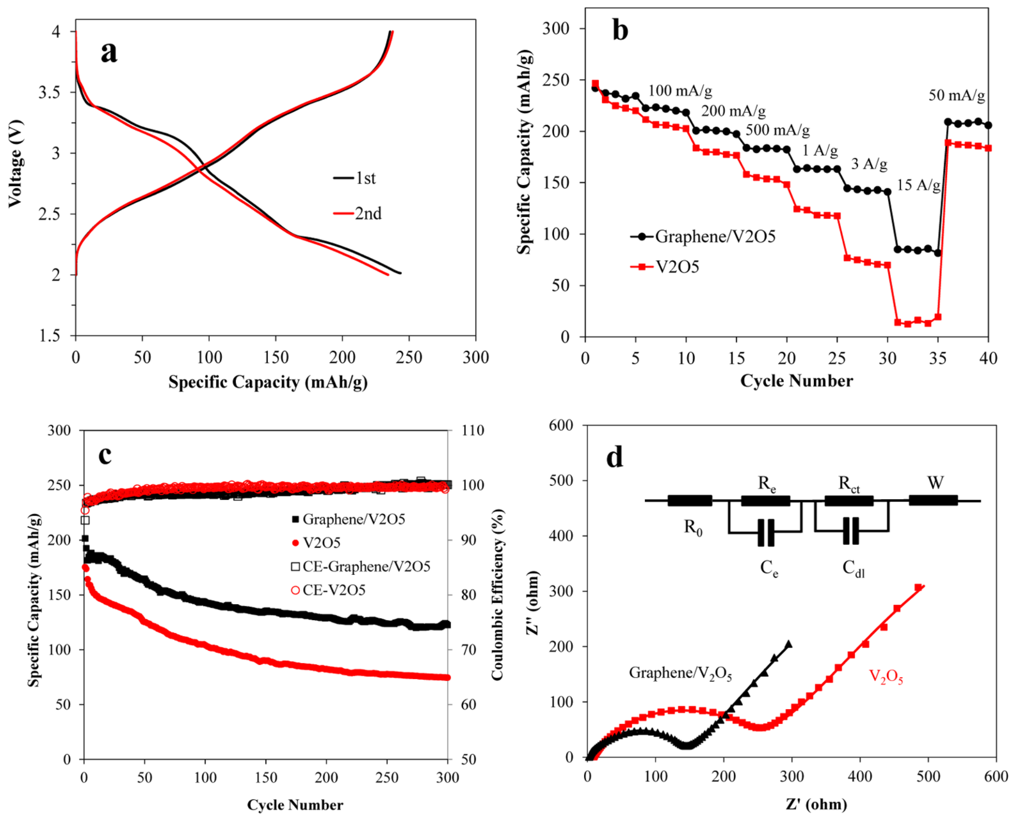

Figure 6. (a) Charge/discharge curves of the graphene/V_2O_5 nanocomposite electrode at a current density of 50 mA/g; (b) rate performance of graphene/V_2O_5 nanocomposites and V_2O_5; (c) capacity retention and Coulombic efficiency of graphene/V_2O_5 nanocomposites and V_2O_5 cycled at 500 mA/g; (d) EIS spectra of graphene/V_2O_5 nanocomposites and V_2O_5.

CV results. The initial discharge and charge capacity based on the total weight of the graphene and the V_2O_5 was ~236 and 243 mAh/g, respectively. Pure graphene was also investigated as electrode materials in LIB cycled between 4 and 2 V, shown in Supporting Information, Figure S3. The specific capacity of graphene was determined to be less than 40 mAh/g, which probably resulted from the double-layer capacitance. As the graphene content in the composites was only 17%, the capacity contributed by graphene would be only ~6 mAh/g. Considering that the wt % of V_2O_5 in the composites was only 83%, the actual specific capacity of V_2O_5 was 277 mAh/g, close to the theoretical capacity of V_2O_5 (294 mAh/g, assuming the intercalation of two lithium ions). The rate performance of the V_2O_5 and the graphene/V_2O_5 nanocomposite is shown in Figure 6b. It can be seen that the specific capacity of the V_2O_5 drops dramatically at high discharge/charge currents. In contrast, the graphene/V_2O_5 nanocomposite shows comparable specific capacity at low current densities and much higher specific capacity at high current densities than the V_2O_5 electrode shows at high current densities. For example, at a high current density of 15 A/g, graphene/V_2O_5 composites still can deliver discharge capacities of 86 mAh/g. However, pure V_2O_5 can hardly be cycled at this current density. This high current density (15 A/g) is comparable with that used in supercapacitors, suggesting superior rate performance for our graphene/V_2O_5 electrode.[40] More importantly, a stable discharge capacity of 209 mAh/g could be recovered when the current was reduced back to 50 mA/g, indicating the excellent electrochemical stability of the graphene/V_2O_5 nanocomposites. The cycling performance was further evaluated by charging/discharging the graphene/V_2O_5 nanocomposite electrode at a current density of 500 mA/g, as shown in Figure 6c. Although some capacity loss upon cycling was observed, the graphene/V_2O_5 nanocomposites exhibited a much slower capacity decay rate than pure V_2O_5. Pure V_2O_5 only delivered ~74 mAh/g after 300 cycles, corresponding to 39% of the initial discharge capacity and approximately 0.2% capacity loss per cycle. In comparison, the graphene/V_2O_5 nanocomposite electrode still maintained a discharge capacity of 122 mAh/g, corresponding to 64% of the initial discharge capacity and approximately 0.12% capacity loss per cycle. The electrode morphology of graphene/V_2O_5 before and after cycling was examined and shown in Supporting Information, Figure S4. No significant change was observed after cycling, suggesting the good structural stability of graphene/V_2O_5. The initial Coulombic efficiency of graphene/V_2O_5 electrode was 93.6%, slightly lower than V_2O_5 electrode (~95.4%). This may be caused by the irreversible Li+ reaction with graphene defects.[41] The Coulombic efficiency increases to 98% after the several cycles and maintained close to 100% during 300 cycles.

To investigate the origin of the enhanced electrochemical performance of the graphene/V_2O_5 nanocomposite, EIS measurements were carried out and are shown in Figure 6d. The EIS spectra were fitted using the equivalent circuit model shown in Figure 6d, where R_0 is the contact resistance, R_e and C_e refer to the resistance and capacitance of the electrode material, respectively, R_{ct} and C_{dl} stand for the charge-transfer resistance and the double-layer capacitance, respectively, and W refers to the Warburg diffusion element.[42] It is shown that the incorporation of graphene in the V_2O_5 caused a decrease in the R_e, from 230.7 Ω in pure V_2O_5 to 71 Ω in graphene/V_2O_5 composites. The charge transfer resistance (R_{ct}) of the graphene/V_2O_5 nanocomposite (15.6 ohm) was also found to be much

dx.doi.org/10.1021/am5047262 | ACS Appl. Mater. Interfaces 2014, 6, 18894−18900

lower than that of pure V_2O_5 (60.1 ohm), indicating improved electrical and ionic conductivity and faster charge transfer in the graphene/V_2O_5 nanocomposites. The Li^+ diffusion coefficient in the graphene/V_2O_5 composites was determined to be ~1.27 × 10^{-12} cm^2/s, higher than that of pure V_2O_5 (1.08 × 10^{-12} cm^2/s). This enhancement could be attributed to the advantages of our hierarchical graphene/V_2O_5 nanocomposite, which has high conductivity, a large specific surface area, and a porous structure.

Overall, the superior electrochemical performance of the graphene/V_2O_5 nanocomposite can be attributed to its unique hierarchical structure resulting from the controlled hydrolysis route. The uniform deposition of V_2O_5 on graphene allows fast electron transfer between the interfaces of the V_2O_5 and graphene. The porous structure of the composites provides rapid electrolyte penetration and a short lithium ion diffusion path within the electrode. The hierarchical structure could effectively prevent structural degradation and delamination of the electrode material from the current collector upon cycling, resulting in an improved cycle life. In addition, the uniform distribution of V_2O_5 on graphene by controlled nucleation process maximized the synergistic interaction between graphene and V_2O_5.

4. CONCLUSIONS

In summary, we report a simple method to prepare V_2O_5 nanosheets or thin film anchored on graphene sheets. Utilizing the synergistic interaction between graphene and V_2O_5, the hierarchical graphene/V_2O_5 nanocomposites possess excellent cycling stability and rate capability when used as the cathode material for lithium-ion batteries. Even charged/discharged at a high current density of 15 A/g, the graphene/V_2O_5 nanocomposite still can deliver discharge capacities of 86 mAh/g. In addition, the graphene/V_2O_5 nanocomposite retained 64% of the initial discharge capacity after 300 cycles at 500 mA/g. This excellent electrochemical performance results from a good electronic conductive path and fast electrolyte ion diffusion due to the uniformly deposited V_2O_5 on the graphene. In addition, the hierarchical structure can effectively prevent the structural degradation of the graphene/V_2O_5 nanocomposites upon cycling. Furthermore, our approach provides an effective strategy to synthesize high-performance nanocomposites.

■ ASSOCIATED CONTENT

Supporting Information

C 1s XPS spectra, SEM image of V_2O_5, capacity retention of graphene, electrode morphology, and tabulated data to compare electrochemical performance from this work with others. This material is available free of charge via the Internet at http://pubs.acs.org.

■ AUTHOR INFORMATION

Corresponding Author

*E-mail: jianxie@iupui.edu.

Notes

The authors declare no competing financial interest.

■ ACKNOWLEDGMENTS

This work was partially supported by the multidisciplinary Undergraduate Research Initiative (MURI) of Indiana University Purdue University Indianapolis (IUPUI). The authors acknowledge Dr. K. Artyushkova at Univ. of New Mexico for the help in XPS experiments. The authors acknowledge Dr. Y. Liu from Argonne National Laboratory for the help with TEM.

■ REFERENCES

(1) Fergus, J. W. Recent developments in cathode materials for lithium ion batteries. *J. Power Sources* **2010**, *195*, 939−954.
(2) Xu, J.; Dou, S.; Liu, H.; Dai, L. Cathode materials for next generation lithium ion batteries. *Nano Energy* **2013**, *2*, 439−442.
(3) Whittingham, M. S. The Role of Ternary Phases in Cathode Reactions. *J. Electrochem. Soc.* **1976**, *123*, 315−320.
(4) Coustier, F.; Passerini, S.; Smyrl, W. H. A 400 mAh/g Aerogel-like V 2 O 5 Cathode for Rechargeable Lithium Batteries. *J. Electrochem. Soc.* **1998**, *145*, L73−L74.
(5) Wang, Y.; Cao, G. Developments in Nanostructured Cathode Materials for High-Performance Lithium-Ion Batteries. *Adv. Mater.* **2008**, *20*, 2251−2269.
(6) Whittingham, M. S.; Song, Y.; Lutta, S.; Zavalij, P. Y.; Chernova, N. A. Some transition metal (oxy)phosphates and vanadium oxides for lithium batteries. *J. Mater. Chem.* **2005**, *15*, 3362−3379.
(7) Wang, Y.; Takahashi, K.; Lee, K. H.; Cao, G. Z. Nanostructured Vanadium Oxide Electrodes for Enhanced Lithium-Ion Intercalation. *Adv. Funct. Mater.* **2006**, *16*, 1133−1144.
(8) Wang, J.; Curtis, C. J.; Schulz, D. L.; Zhang, J.-G. Influences of Treatment Temperature and Water Content on Capacity and Rechargeability of V 2 O 5 Xerogel Films. *J. Electrochem. Soc.* **2004**, *151*, A1−A7.
(9) Baddour-Hadjean, R.; Pereira-Ramos, J. P.; Navone, C.; Smirnov, M. Raman Microspectrometry Study of Electrochemical Lithium Intercalation into Sputtered Crystalline V2O5 Thin Films. *Chem. Mater.* **2008**, *20*, 1916−1923.
(10) Liu, Q.; Liu, Y.; Sun, C.-J.; Li, Z.-f.; Ren, Y.; Lu, W.; Stach, E. A.; Xie, J. The Structural Evolution of V2O5 Nanocystals during Electrochemical Cycling Studied Using In operando Synchrotron Techniques. *Electrochim. Acta* **2014**, *136*, 318−322.
(11) Yu, D.; Chen, C.; Xie, S.; Liu, Y.; Park, K.; Zhou, X.; Zhang, Q.; Li, J.; Cao, G. Mesoporous vanadium pentoxide nanofibers with significantly enhanced Li-ion storage properties by electrospinning. *Energy Environ. Sci.* **2011**, *4*, 858−861.
(12) Wang, Y.; Takahashi, K.; Shang, H.; Cao, G. Synthesis and Electrochemical Properties of Vanadium Pentoxide Nanotube Arrays. *J. Phys. Chem. B* **2005**, *109*, 3085−3088.
(13) Rui, X.; Lu, Z.; Yu, H.; Yang, D.; Hng, H. H.; Lim, T. M.; Yan, Q. Ultrathin V2O5 nanosheet cathodes: realizing ultrafast reversible lithium storage. *Nanoscale* **2013**, *5*, 556−560.
(14) Pan, A. Q.; Wu, H. B.; Zhang, L.; Lou, X. W. Uniform V2O5 nanosheet-assembled hollow microflowers with excellent lithium storage properties. *Energy Environ. Sci.* **2013**, *6*, 1476−1479.
(15) Wu, H. B.; Pan, A.; Hng, H. H.; Lou, X. W. Template-Assisted Formation of Rattle-type V2O5 Hollow Microspheres with Enhanced Lithium Storage Properties. *Adv. Funct. Mater.* **2013**, *23*, 5669−5674.
(16) Zhao, Y.; Peng, L.; Liu, B.; Yu, G. Single-Crystalline LiFePO4 Nanosheets for High-Rate Li-Ion Batteries. *Nano Lett.* **2014**, *14*, 2849−2853.
(17) Wu, C.; Lu, X.; Peng, L.; Xu, K.; Peng, X.; Huang, J.; Yu, G.; Xie, Y. Two-dimensional vanadyl phosphate ultrathin nanosheets for high energy density and flexible pseudocapacitors. *Nat. Commun.* **2013**, *4*.
(18) Koltypin, M.; Pol, V.; Gedanken, A.; Aurbach, D. The Study of Carbon-Coated V2O5 Nanoparticles as a Potential Cathodic Material for Li Rechargeable Batteries. *J. Electrochem. Soc.* **2007**, *154*, A605−A613.
(19) Zhou, X.; Wu, G.; Wu, J.; Yang, H.; Wang, J.; Gao, G.; Cai, R.; Yan, Q. Multiwalled carbon nanotubes-V2O5 integrated composite with nanosized architecture as a cathode material for high performance lithium ion batteries. *J. Mater. Chem. A* **2013**, *1*, 15459−15468.
(20) Sathiya, M.; Prakash, A. S.; Ramesha, K.; Tarascon, J. M.; Shukla, A. K. V2O5-Anchored Carbon Nanotubes for Enhanced Electrochemical Energy Storage. *J. Am. Chem. Soc.* **2011**, *133*, 16291−16299.
(21) Zhang, X.-F.; Wang, K.-X.; Wei, X.; Chen, J.-S. Carbon-Coated V2O5 Nanocrystals as High Performance Cathode Material for Lithium Ion Batteries. *Chem. Mater.* **2011**, *23*, 5290−5292.
(22) Allen, M. J.; Tung, V. C.; Kaner, R. B. Honeycomb Carbon: A Review of Graphene. *Chem. Rev.* **2009**, *110*, 132−145.

(23) Rui, X.; Zhu, J.; Sim, D.; Xu, C.; Zeng, Y.; Hng, H. H.; Lim, T. M.; Yan, Q. Reduced graphene oxide supported highly porous V2O5 spheres as a high-power cathode material for lithium ion batteries. *Nanoscale* **2011**, *3*, 4752−4758.
(24) Liu, H.; Yang, W. Ultralong single crystalline V2O5 nanowire/graphene composite fabricated by a facile green approach and its lithium storage behavior. *Energy Environ. Sci.* **2011**, *4*, 4000−4008.
(25) Du, G.; Seng, K. H.; Guo, Z.; Liu, J.; Li, W.; Jia, D.; Cook, C.; Liu, Z.; Liu, H. Graphene-V2O5[middle dot]nH2O xerogel composite cathodes for lithium ion batteries. *RSC Adv.* **2011**, *1*, 690−697.
(26) Sun, Y.; Yang, S.-B.; Lv, L.-P.; Lieberwirth, I.; Zhang, L.-C.; Ding, C.-X.; Chen, C.-H. A composite film of reduced graphene oxide modified vanadium oxide nanoribbons as a free standing cathode material for rechargeable lithium batteries. *J. Power Sources* **2013**, *241*, 168−172.
(27) Cheng, J.; Wang, B.; Xin, H. L.; Yang, G.; Cai, H.; Nie, F.; Huang, H. Self-assembled V2O5 nanosheets/reduced graphene oxide hierarchical nanocomposite as a high-performance cathode material for lithium ion batteries. *J. Mater. Chem. A* **2013**, *1*, 10814−10820.
(28) Li, Z.-F.; Zhang, H.; Liu, Q.; Liu, Y.; Stanciu, L.; Xie, J. Covalently-grafted polyaniline on graphene oxide sheets for high performance electrochemical supercapacitors. *Carbon* **2014**, *71*, 257−267.
(29) Li, Z.-F.; Zhang, H.; Liu, Q.; Liu, Y.; Stanciu, L.; Xie, J. Novel Pyrolyzed Polyaniline-Grafted Silicon Nanoparticles Encapsulated in Graphene Sheets As Li-Ion Battery Anodes. *ACS Appl. Mater. Interfaces* **2014**, *6*, 5996−6002.
(30) Kijenski, J.; Baiker, A.; Glinski, M.; Dollenmeier, P.; Wokaun, A. Monolayers and double layers of vanadium pentoxide on different carriers: Preparation, characterization and catalytic activities. *J. Catal.* **1986**, *101*, 1−11.
(31) Wang, Z.-l.; Xu, D.; Huang, Y.; Wu, Z.; Wang, L.-m.; Zhang, X.-b. Facile, mild and fast thermal-decomposition reduction of graphene oxide in air and its application in high-performance lithium batteries. *Chem. Commun.* **2012**, *48*, 976−978.
(32) Vadivel Murugan, A. Novel organic−inorganic poly (3,4-ethylenedioxythiophene) based nanohybrid materials for rechargeable lithium batteries and supercapacitors. *J. Power Sources* **2006**, *159*, 312−318.
(33) Markad, G. B.; Battu, S.; Kapoor, S.; Haram, S. K. Interaction between Quantum Dots of CdTe and Reduced Graphene Oxide: Investigation through Cyclic Voltammetry and Spectroscopy. *J. Phys. Chem. C* **2013**, *117*, 20944−20950.
(34) Li, X.; Tay, B.; Li, J.; Tan, D.; Tan, C.; Liang, K. Mildly reduced graphene oxide-Ag nanoparticle hybrid films for surface-enhanced Raman scattering. *Nanoscale Res. Lett.* **2012**, *7*, 1−8.
(35) Li, Y.; Yao, J.; Uchaker, E.; Zhang, M.; Tian, J.; Liu, X.; Cao, G. Sn-Doped V2O5 Film with Enhanced Lithium-Ion Storage Performance. *J. Phys. Chem. C* **2013**, *117*, 23507−23514.
(36) Chan, C. K.; Peng, H.; Twesten, R. D.; Jarausch, K.; Zhang, X. F.; Cui, Y. Fast, Completely Reversible Li Insertion in Vanadium Pentoxide Nanoribbons. *Nano Lett.* **2007**, *7*, 490−495.
(37) Ding, S.; Luan, D.; Boey, F. Y. C.; Chen, J. S.; Lou, X. W. SnO2 nanosheets grown on graphene sheets with enhanced lithium storage properties. *Chem. Commun.* **2011**, *47*, 7155−7157.
(38) Huang, S.-Z.; Cai, Y.; Jin, J.; Li, Y.; Zheng, X.-F.; Wang, H.-E.; Wu, M.; Chen, L.-H.; Su, B.-L. Annealed vanadium oxide nanowires and nanotubes as high performance cathode materials for lithium ion batteries. *J. Mater. Chem. A* **2014**, *2*, 14099−14108.
(39) Park, H. K.; Smyrl, W. H.; Ward, M. D. V 2 O 5 Xerogel Films as Intercalation Hosts for Lithium: I. Insertion Stoichiometry, Site Concentration, and Specific Energy. *J. Electrochem. Soc.* **1995**, *142*, 1068−1073.
(40) Zhang, L. L.; Zhao, X. S. Carbon-based materials as supercapacitor electrodes. *Chem. Soc. Rev.* **2009**, *38*, 2520−2531.
(41) Wu, Z.-S.; Ren, W.; Xu, L.; Li, F.; Cheng, H.-M. Doped Graphene Sheets As Anode Materials with Superhigh Rate and Large Capacity for Lithium Ion Batteries. *ACS Nano* **2011**, *5*, 5463−5471.
(42) Liu, Y.; Liu, Q.; Li, Z.; Ren, Y.; Xie, J.; He, H.; Xu, F. Failure Study of Commercial LiFePO4 Cells in over-Discharge Conditions Using Electrochemical Impedance Spectroscopy. *J. Electrochem. Soc.* **2014**, *161*, A620−A632.